Electronic Supplementary Information (ESI)

Bidirectional Photoswitching of Magnetic Properties at Room Temperature: Ligand-Driven Light-Induced Valence Tautomerism

Alexander Witt, Frank W. Heinemann, and Marat M. Khusniyarov*

Friedrich-Alexander-University of Erlangen-Nuremberg
Department of Chemistry and Pharmacy
Egerlandstr. 1, 91058 Erlangen
Germany

*e-mail: marat.khusniyarov@fau.de

Evaluation of variable-temperature data

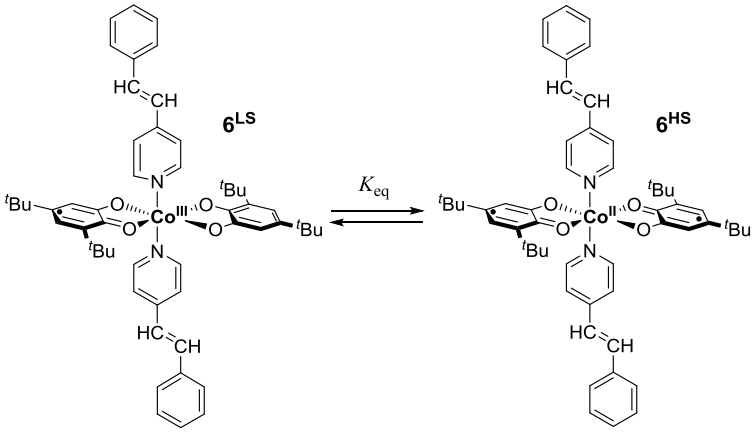

Scheme S1. Valence tautomeric (VT) equilibrium between redox isomers *trans*-**6**$^{\mathbf{LS}}$ and *trans*-**6**$^{\mathbf{HS}}$.

Variable-temperature magnetic susceptibility data and variable-temperature electronic absorption spectra for *trans*-**6** and *cis*-**6** were fitted using expressions eq. (2) and eq. (3), respectively, derived from the van't Hoff equation eq. (1). The following quantities are used: equilibrium constant K_{eq} (Scheme S1), enthalpy change ΔH and entropy change ΔS for the equilibrium reaction, observed effective magnetic moment μ_{eff}, the high- and low-temperature limits of magnetic moment μ_{eff}(HT) and μ_{eff}(LT), respectively, observed absorption A_{obs}, the high- and low-temperature limits of absorption A(HT) and A(LT).

$$\ln K_{eq} = -\frac{\Delta H}{RT} + \frac{\Delta S}{R} \tag{1}$$

$$\mu_{eff} = \sqrt{\frac{e^{\left(-\frac{\Delta H}{RT}+\frac{\Delta S}{R}\right)}\mu_{eff}^2(\mathrm{HT}) + \mu_{eff}^2(\mathrm{LT})}{e^{\left(-\frac{\Delta H}{RT}+\frac{\Delta S}{R}\right)}+1}} \tag{2}$$

$$A_{obs} = \frac{e^{\left(-\frac{\Delta H}{RT}+\frac{\Delta S}{R}\right)}A(\mathrm{HT}) + A(\mathrm{LT})}{e^{\left(-\frac{\Delta H}{RT}+\frac{\Delta S}{R}\right)}+1} \tag{3}$$

Titration with 4-stypy and derivation of fitting functions

In ligand titration experiments monitored by the Evans ^{1}H NMR method, the outer and inner tubes contained solutions with equal amounts of added ligand. The diamagnetic corrections for *trans*-**6** as well as *cis*-**6** were determined from Pascal's constants ($\chi_{dia} = -5.45 \cdot 10^{-4}$ emu mol^{-1}).[1] Sample preparation and data collection were both performed under strictly anaerobic conditions. The following considerations are applied: **6** = *trans*-**6** or *cis*-**6**, $\mathbf{6^{LS}}$ = *trans*-$\mathbf{6^{LS}}$ or *cis*-$\mathbf{6^{LS}}$, $\mathbf{6^{HS}}$ = *trans*-$\mathbf{6^{HS}}$ or *cis*-$\mathbf{6^{HS}}$, and **5** = *trans*-**5** or *cis*-**5**.

We can reasonably assume that a solution of **6** at RT contains three cobalt species in equilibrium: a six-coordinate low-spin cobalt(III) species $\mathbf{6^{LS}}$, a six-coordinate high-spin cobalt(II) species $\mathbf{6^{HS}}$, and a five-coordinate high-spin cobalt(II) species **5** (eq. (4)). The presence of hypothetic four-coordinate species can be ruled out since they are not thermodynamically stable in solution and build tetramers,[2] which we did not observe.

$$\mathbf{5} \underset{-\text{ 4-stypy}}{\overset{K_a}{\underset{+\text{ 4-stypy}}{\rightleftharpoons}}} \left\{ \mathbf{6^{LS}} \overset{K_{eq}}{\rightleftharpoons} \mathbf{6^{HS}} \right\} \tag{4}$$

Upon addition of 4-*stypy* (t*rans*- or *cis*-) to the appropriate complex solution the equilibrium is shifted towards the six-coordinate species $\mathbf{6^{LS}}$ and $\mathbf{6^{HS}}$ according to eq. (4).

The VT equilibrium between redox isomers $\mathbf{6^{LS}}$ and $\mathbf{6^{HS}}$ depends on temperature, however the ratio between the redox isomers remains constant at constant (room) temperature regardless of 4-*stypy* concentration (eq. (5)).

$$\left.\frac{[\mathbf{6^{HS}}]}{[\mathbf{6^{LS}}]}\right|_{T=\text{const.}} = K_{eq} \tag{5}$$

Therefore, $\mathbf{6^{LS}}$ and $\mathbf{6^{HS}}$ can be taken as a six-coordinate pseudo-species $\mathbf{6} \equiv \{\mathbf{6^{HS}} \leftrightarrow \mathbf{6^{LS}}\}$, the concentration of which is increased upon titration with 4-*stypy*. This assumption is strongly supported by the observation of an isosbestic point in a series of electronic spectra upon titration. The association constant K_a is defined as:

$$K_a = \frac{[\mathbf{6}]}{[\mathbf{5}] \cdot [\mathrm{L}]} \tag{6}$$

, where L = 4-*stypy*.

Then the total concentration of cobalt species $[\mathrm{Co}]_t$ (**6** + **5**) and 4-*stypy* ligand $[\mathrm{L}]_t$ (associated + dissociated) can be expressed as:

$$[\mathbf{6}] + [\mathbf{5}] = [\mathrm{Co}]_t \tag{7}$$

$$[\mathbf{6}] + [\mathrm{L}] = [\mathrm{L}]_t \tag{8}$$

By substituting [**5**] and [L] in eq. (6) with eq. (7) and eq. (8), we obtain

$$K_a = \frac{[\mathbf{6}]}{([\mathrm{Co}]_t - [\mathbf{6}]) \cdot ([\mathrm{L}]_t - [\mathbf{6}])} \tag{9}$$

Given the observed (total) *molar* magnetic susceptibility of solution, χ_{obs}, is the *weighted* sum of the molar magnetic susceptibilities of five-coordinate species **5**, $\chi(\mathbf{5})$, and six-coordinate quasi-species **6**, $\chi(\mathbf{6})$, which is composed of $\chi(\mathbf{6^{LS}})$ and $\chi(\mathbf{6^{HS}})$, χ_{obs} can be expressed as

$$\chi_{obs} = \chi(\mathbf{6})\frac{[\mathbf{6}]}{[\mathrm{Co}]_t} + \chi(\mathbf{5})\left(1 - \frac{[\mathbf{6}]}{[\mathrm{Co}]_t}\right) = \frac{[\mathbf{6}]}{[\mathrm{Co}]_t}(\chi(\mathbf{6}) - \chi(\mathbf{5})) + \chi(\mathbf{5}) \tag{10}$$

Eq. (10) can be solved and substituted for [**6**] in eq. (9) to give the final eq. (11) that was used to fit the magnetic susceptibility of solution χ_{obs} as a function of ligand concentration $[\mathrm{L}]_t$.

$$\chi_{obs} = \frac{(\chi(\mathbf{5}) - \chi(\mathbf{6}))\sqrt{[\mathrm{Co}]_t^2 K_a^2 - 2[\mathrm{Co}]_t K_a^2 [\mathrm{L}]_t + 2[\mathrm{Co}]_t K_a + K_a^2 [\mathrm{L}]_t^2 + 2K_a[\mathrm{L}]_t + 1} - [\mathrm{Co}]_t \chi(\mathbf{5}) K_a - [\mathrm{Co}]_t \chi(\mathbf{6}) K_a + \chi(\mathbf{5}) K_a [\mathrm{L}]_t - \chi(\mathbf{6}) K_a [\mathrm{L}]_t + \chi(\mathbf{5}) - \chi(\mathbf{6})}{2[\mathrm{Co}]_t K_a} \tag{11}$$

Similarly, the dependence of the 750 nm absorption band on the amount of added 4-*stypy* ligand can be derived:

Since free 4-*stypy* does not contribute to the absorption at 750 nm, the observed (total) absorption, A_{obs}, is the sum of the respective absorptions of **5**, $\mathbf{6^{HS}}$, and $\mathbf{6^{LS}}$. Since the temperature was kept constant, the ratio between $\mathbf{6^{HS}}$ and $\mathbf{6^{LS}}$ remains unchanged during titration. Hence, the shift in the equilibrium between **5** and a quasi-species $\mathbf{6} \equiv \{\mathbf{6^{HS}} \leftrightarrow \mathbf{6^{LS}}\}$ can be described with molar extinction coefficients $\varepsilon(\mathbf{5})$ and $\varepsilon(\mathbf{6})$ respectively:

$$A_{obs} = \varepsilon(\mathbf{6})[\mathbf{6}] + \varepsilon(\mathbf{5})[\mathbf{5}] = \varepsilon(\mathbf{5})([\mathrm{Co}]_t - [\mathbf{5}]) + \varepsilon(\mathbf{6})[\mathbf{6}] = [\mathbf{6}](\varepsilon(\mathbf{6}) - \varepsilon(\mathbf{5})) + \varepsilon(\mathbf{5})[\mathrm{Co}]_t \tag{12}$$

Eq. (12) can be solved and substituted for [**6**] in eq. (9) to yield the final eq. (13) that was used to fit the absorption at 750 nm, A_{obs}, as a function of ligand concentration $[\mathrm{L}]_t$:

$$A_{obs} = \frac{(\varepsilon(\mathbf{5}) - \varepsilon(\mathbf{6}))\sqrt{[\mathrm{Co}]_t^2 K_a^2 - 2[\mathrm{Co}]_t K_a^2 [\mathrm{L}]_t + 2[\mathrm{Co}]_t K_a + K_a^2 [\mathrm{L}]_t^2 + 2K_a[\mathrm{L}]_t + 1} + [\mathrm{Co}]_t \varepsilon(\mathbf{5}) K_a + [\mathrm{Co}]_t \varepsilon(\mathbf{6}) K_a - \varepsilon(\mathbf{5}) K_a [\mathrm{L}]_t + \varepsilon(\mathbf{6}) K_a [\mathrm{L}]_t - \varepsilon(\mathbf{5}) + \varepsilon(\mathbf{6})}{2K_a} \tag{13}$$

The degree of dissociation defined as

$$\alpha = 100\% \frac{[\mathbf{5}]}{[\mathbf{5}] + [\mathbf{6}]} \tag{14}$$

can be easily calculated via

$$\alpha = 100\% \cdot \frac{-1 + \sqrt{1 + 4K_a[\mathrm{Co}]_t}}{2K_a[\mathrm{Co}]_t} \tag{15}$$

Figures and tables

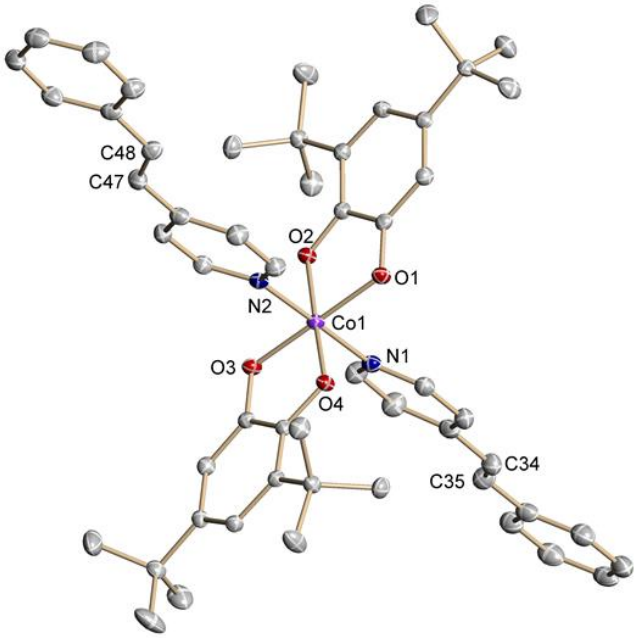

Figure S1. Molecular structure of *trans*-**6** determined at 120 K. Thermal ellipsoids are drawn at 50 % probability. Hydrogen atoms are omitted for clarity.

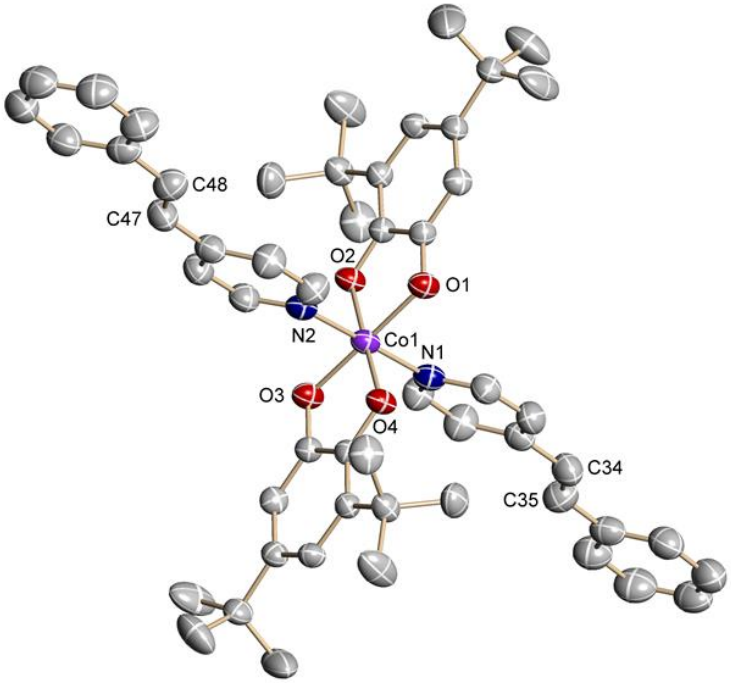

Figure S2. Molecular structure of *trans*-**6** determined at 295 K. Thermal ellipsoids are drawn at 50 % probability. Hydrogen atoms are omitted for clarity.

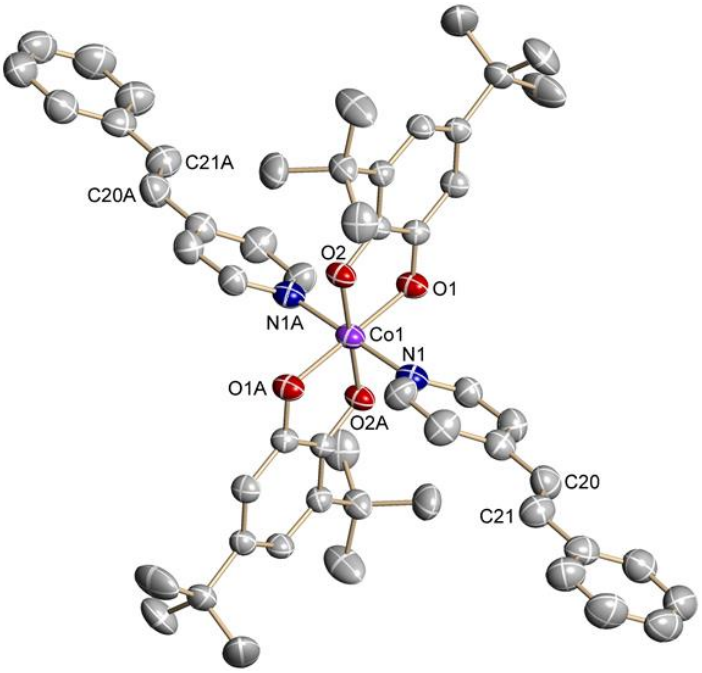

Figure S3. Molecular structure of *trans*-**6** determined at 305 K. Thermal ellipsoids are drawn at 50 % probability. Hydrogen atoms are omitted for clarity.

Table S1. Selected bond lengths [Å] of *trans*-**6** determined by X-ray crystallography at 120 and 295 K.

	120 K	295 K
Co1–N1	1.938(1)	1.933(5)
Co1–N2	1.945(1)	1.925(5)
Co1–O1	1.910(1)	1.904(1)
Co1–O2	1.916(1)	1.902(1)
Co1–O3	1.863(1)	1.867(1)
Co1–O4	1.854(1)	1.867(1)
C1–O1	1.300(2)	1.304(2)
C6–O2	1.297(2)	1.298(2)
C15–O3	1.349(2)	1.342(2)
C20–O4	1.354(2)	1.342(2)
C1–C6	1.443(2)	1.444(2)
C1–C2	1.409(2)	1.400(2)
C2–C3	1.373(2)	1.371(2)
C3–C4	1.431(2)	1.425(2)
C4–C5	1.372(2)	1.371(2)
C5–C6	1.435(2)	1.425(2)
C15–C20	1.412(2)	1.415(2)
C15–C16	1.390(2)	1.385(2)
C16–C17	1.397(2)	1.388(2)
C17–C18	1.393(2)	1.402(2)
C18–C19	1.405(2)	1.392(2)
C19–C20	1.400(2)	1.406(2)

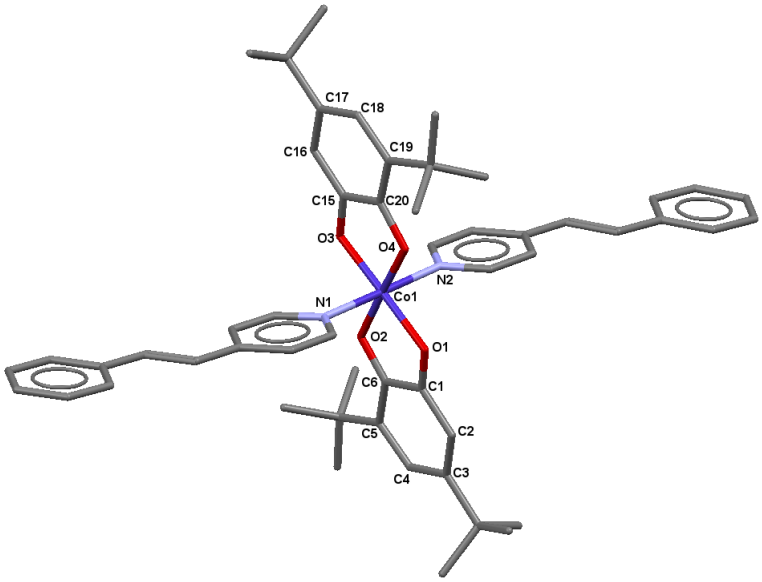

Table S2. Selected bond lengths [Å] of *trans*-**6** determined by X-ray crystallography at 305 K.

	305 K
Co1–N1	1.912(5)
Co1–O1	1.886(1)
Co1–O2	1.887(1)
C1–O1	1.324(2)
C6–O2	1.323(2)
C1–C6	1.426(2)
C1–C2	1.394(2)
C2–C3	1.382(2)
C3–C4	1.409(2)
C4–C5	1.382(2)
C5–C6	1.416(2)

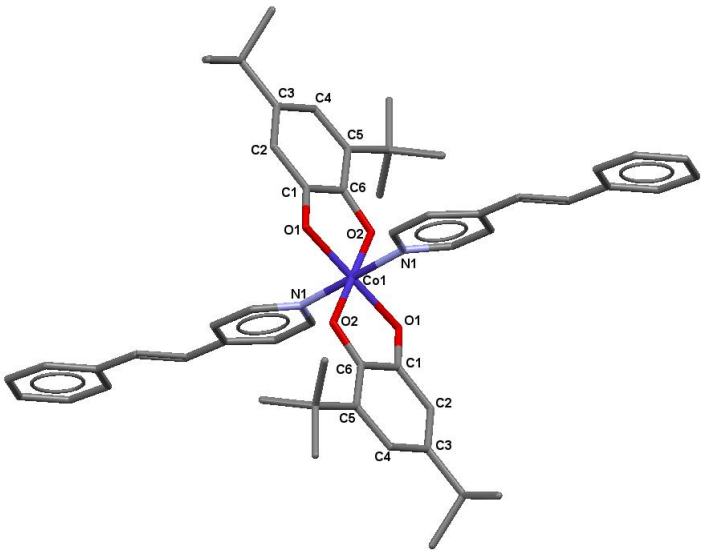

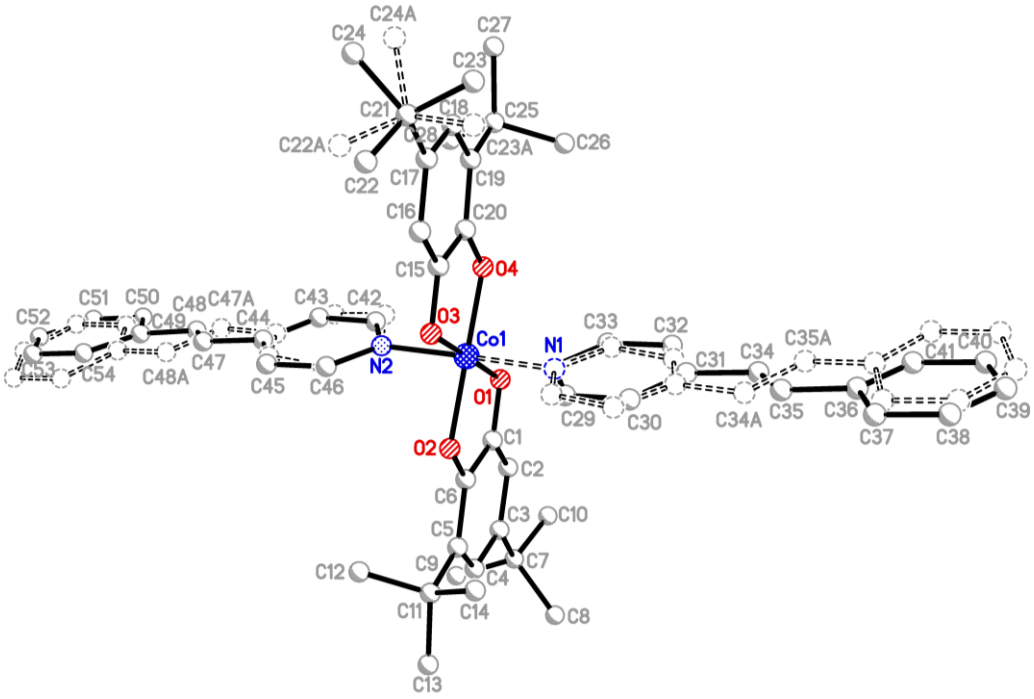

Figure S4. Two alternative orientations of *trans*-4-stypy ligands in *trans*-**6** at 295 K featuring inverted orientations of the ethylene bond. Refinement resulted in site occupancies of 85.4(3) and 14.6(3) % of the 50 involved atoms.

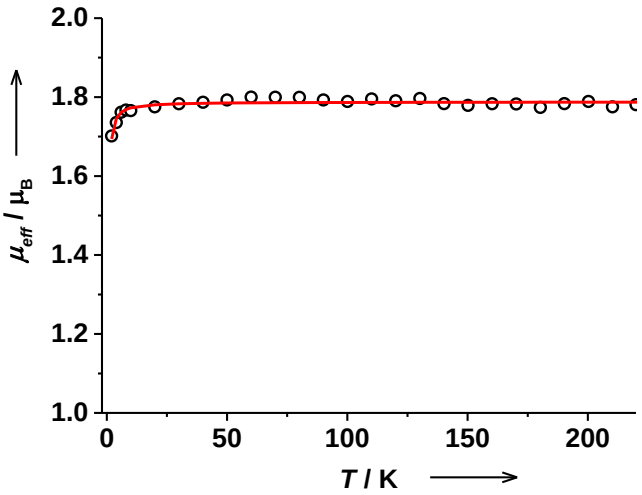

Figure S5. Temperature dependent effective magnetic moment measured on a microcrystalline sample of *trans*-**6** at external magnetic field of 1 T. Low temperature region is shown. Fit parameters for data points in the range 2 – 220 K: $S = 1/2$, $g = 2.064$, $\Theta = -0.15$ K.

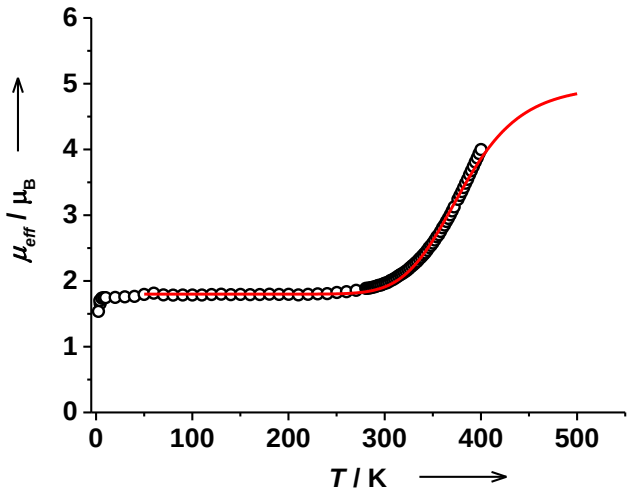

Figure S6. Temperature dependent effective magnetic moment measured on a microcrystalline sample of *trans*-**6** at external magnetic field of 1 T. Van´t Hoff fit parameters: enthalpy change ΔH = 41(1) kJ mol^{-1}, entropy change ΔS = 104(3) J mol^{-1} K^{-1}; low-temperature effective magnetic moment μ_{eff}(LT) = 1.80(1) μ_B. The high-temperature magnetic moment μ_{eff}(HT) was fixed at 5.0 μ_B. Estimated transition temperature: $T_{1/2}$ = 394 K.

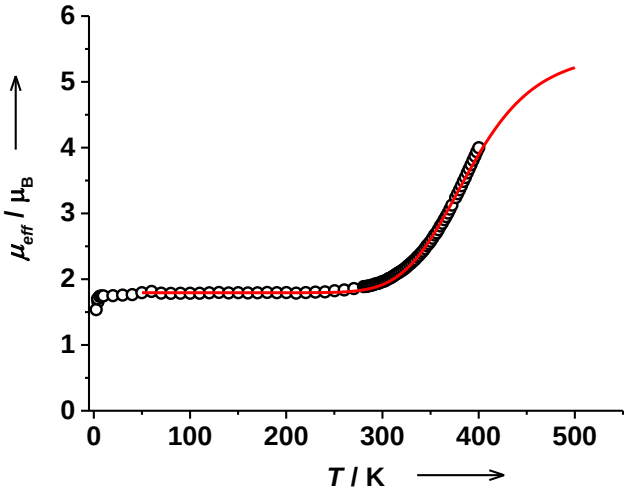

Figure S7. Temperature dependent effective magnetic moment measured on a microcrystalline sample of *trans*-**6** at external magnetic field of 1 T. Alternative van´t Hoff fit: ΔH = 38(1) kJ mol^{-1}, ΔS = 94(2) J mol^{-1} K^{-1}; low-temperature effective magnetic moment: μ_{eff}(LT) = 1.79(1) μ_B. The high-temperature magnetic moment μ_{eff}(HT) was fixed at 5.5 μ_B. Estimated transition temperature: $T_{1/2}$ = 404 K.

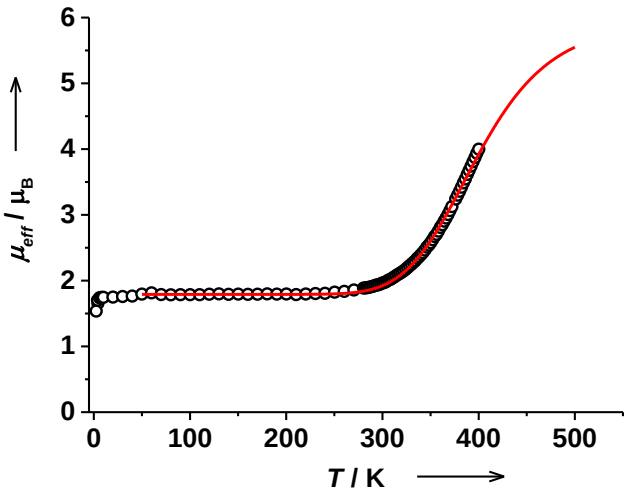

Figure S8. Temperature dependent effective magnetic moment measured on a microcrystalline sample of *trans*-**6** at external magnetic field of 1 T. Alternative van´t Hoff fit: ΔH = 37(1) kJ mol^{-1} , ΔS = 87(2) J mol^{-1} K^{-1}; low-temperature effective magnetic moment: μ_{eff}(LT) = 1.79(1) μ_B. The high-temperature magnetic moment μ_{eff}(HT) was fixed at 6.0 μ_B. Estimated transition temperature: $T_{1/2}$ = 425 K.

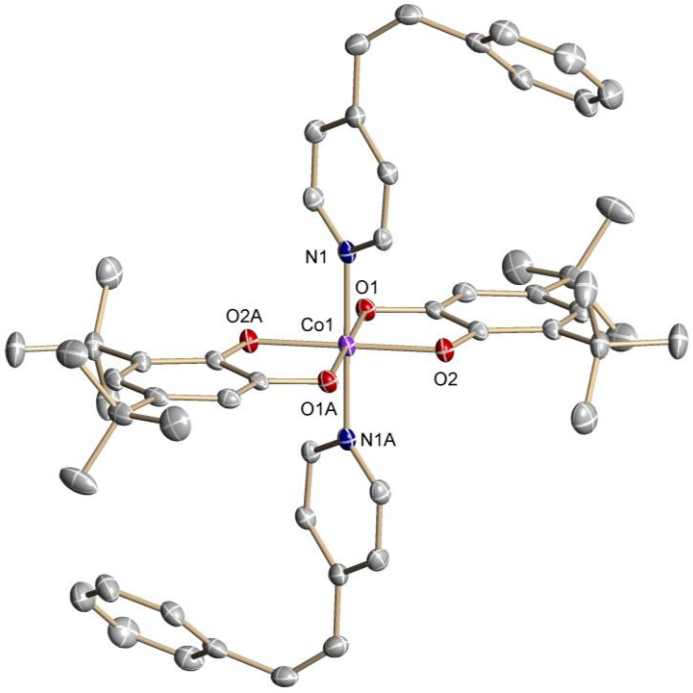

Figure S9. Molecular structure of *cis*-**6** determined at 100 K. Thermal ellipsoids are drawn at 50 % probability. Hydrogen atoms are omitted for clarity.

Table S3. Selected bond lengths [Å] of *cis*-**6** determined by X-ray crystallography at 100 K.

	100 K
Co1–N1	1.940(1)
Co1–O1	1.885(1)
Co1–O2	1.878(1)
C1–O1	1.326(2)
C6–O2	1.326(2)
C1–C6	1.427(2)
C1–C2	1.403(2)
C2–C3	1.385(2)
C3–C4	1.414(2)
C4–C5	1.392(2)
C5–C6	1.418(2)

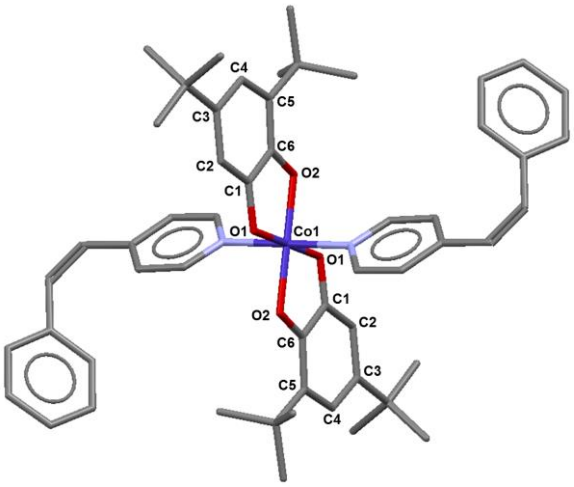

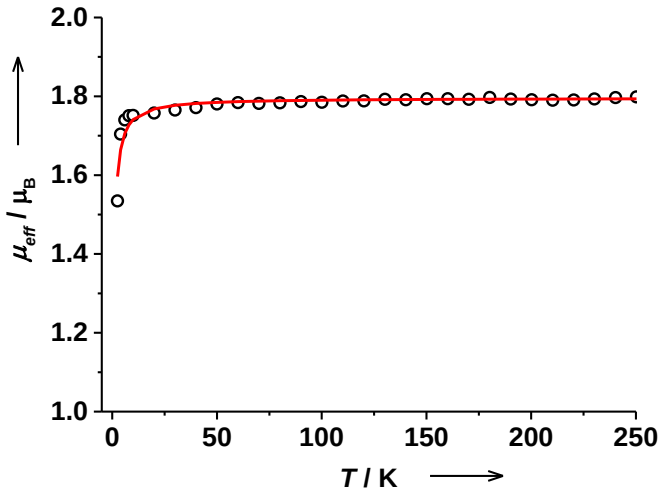

Figure S10. Temperature dependent effective magnetic moment measured on a microcrystalline sample of *cis*-**6** at external magnetic field of 1 T. Low temperature region is shown. Fit parameters for data points in the range 2 – 250 K: $S = 1/2$, $g = 2.073$, $\Theta = -0.62$ K.

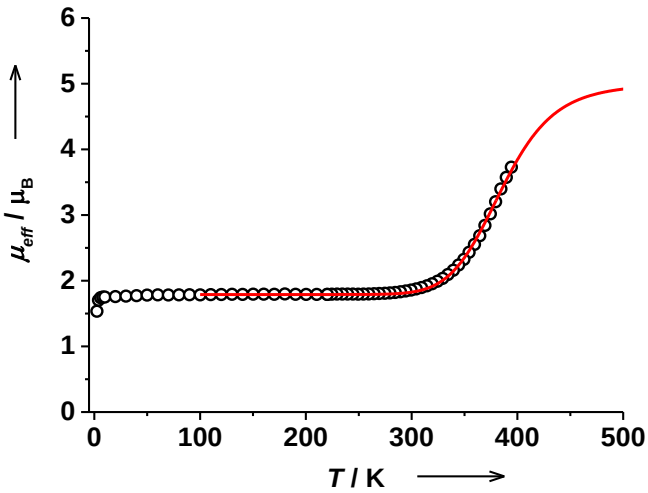

Figure S11. Temperature dependent effective magnetic moment measured on a microcrystalline sample of *cis*-**6** at external magnetic field of 1 T. Van´t Hoff fit parameters: enthalpy change $\Delta H = 52(2)$ kJ mol^{-1}, entropy change $\Delta S = 131(3)$ J mol^{-1} K^{-1}; low-temperature effective magnetic moment μ_{eff}(LT) = 1.79(1) μ_B. The high-temperature magnetic moment μ_{eff}(HT) was fixed at 5.0 μ_B. Estimated transition temperature: $T_{1/2}$ = 397 K.

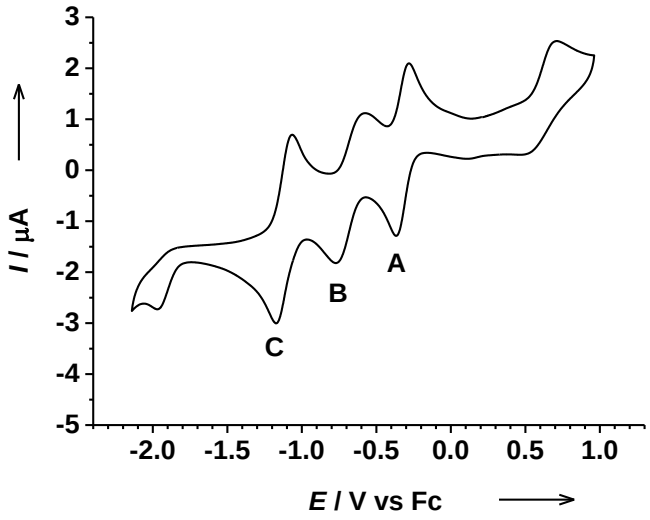

Figure S12. Cyclic voltammogram of *trans*-**6** dissolved in CH_2Cl_2 containing $^{n}Bu_4NPF_6$ (0.1 M) as supporting electrolyte (room temperature, scan rate 25 mV s^{-1}).

Table S4. Electrochemical data for *trans*-**6** dissolved in dichloromethane obtained from a cyclic voltammogram recorded at room temperature at a scan rate 25 mV s^{-1}. All potentials are referenced versus the Fc/Fc^{+} couple.

redox process	E_{pc}, V	E_{pa}, V	$\lvert\Delta E_p\rvert$, V	$E_{1/2}$, V	i_{pc}, µA	i_{pa}, µA	$\lvert i_{pc} / i_{pa}\rvert$
A	–0.28	–0.37	0.09	–0.33	+1.32	–1.60	0.83
B	–0.57	–0.77	0.20	–0.67	+1.17	–1.24	0.94
C	–1.06	–1.17	0.11	–1.12	+1.85	–1.65	1.12

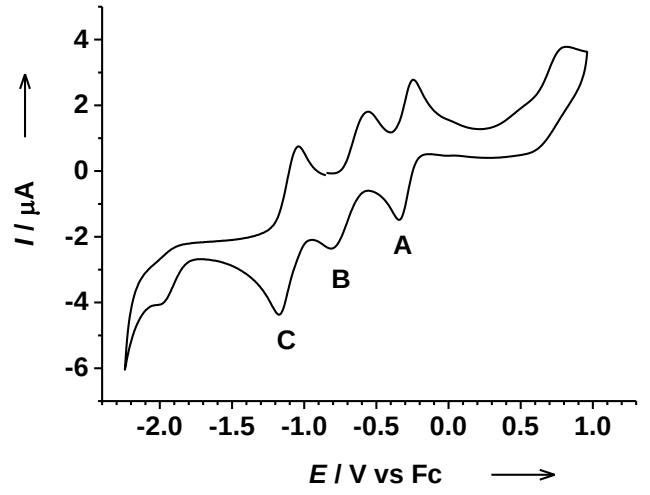

Figure S13. Cyclic voltammogram of *cis*-**6** dissolved in CH_2Cl_2 containing $^{n}Bu_4NPF_6$ (0.1 M) as supporting electrolyte (room temperature, scan rate 25 mV s^{-1}).

Table S5. Electrochemical data for *cis*-**6** dissolved in dichloromethane obtained from a cyclic voltammogram recorded at room temperature at a scan rate 25 mV s^{-1}. All potentials are referenced versus the Fc/Fc^{+} couple.

redox process	E_{pc}, V	E_{pa}, V	$\lvert\Delta E_p\rvert$, V	$E_{1/2}$, V	i_{pc}, µA	i_{pa}, µA	$\lvert i_{pc} / i_{pa}\rvert$
A	–0.24	–0.34	0.10	–0.29	+1.39	–1.63	0.85
B	–0.56	–0.81	0.25	–0.69	+1.22	–1.27	0.96
C	–1.04	–1.17	0.13	–1.11	+1.89	–1.80	1.05

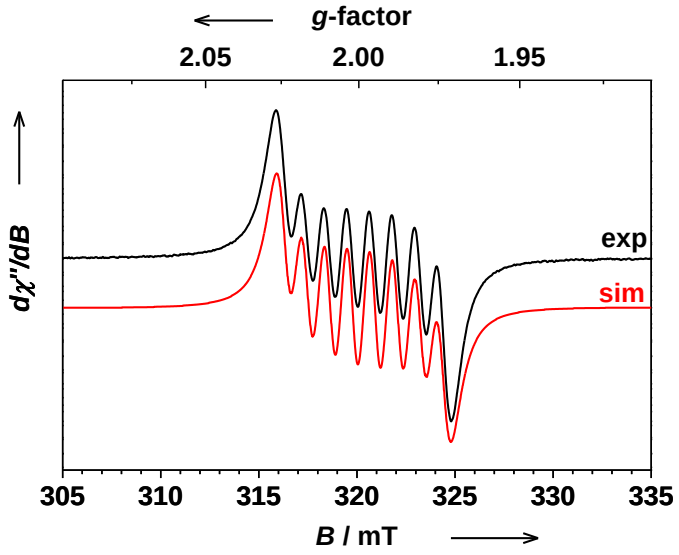

Figure S14. X-band EPR spectrum of *trans*-**6** in CH_2Cl_2 (c = 1.2×10^{-3} M) recorded at room temperature (frequency: 8.9587 GHz; modulation: 0.4 mT; power: 1.0 mW). Fit parameters: g_{iso} = 1.9980, A_{iso}(^{59}Co, I = 7/2) = 1.07×10^{-3} cm^{-1}. Experimental spectrum is depicted by the black trace and simulation is shown in red.

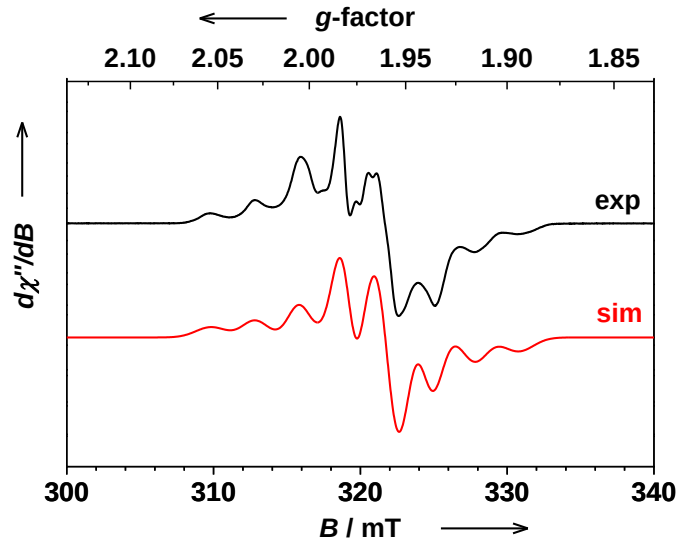

Figure S15. X-band EPR spectrum of *trans*-**6** dissolved in toluene and recorded at 14 K (frequency: 8.9760 GHz; modulation: 0.5 mT; power: 1.0 mW). Fit parameters: $\boldsymbol{g}$ = (1.9887, 2.0022, 2.0051), $\boldsymbol{A}$(^{59}Co, I = 7/2) = (0.4, 28.1, 3.9)×10^{-4} cm^{-1}. Experimental spectrum is depicted by the black trace and simulation is shown in red.

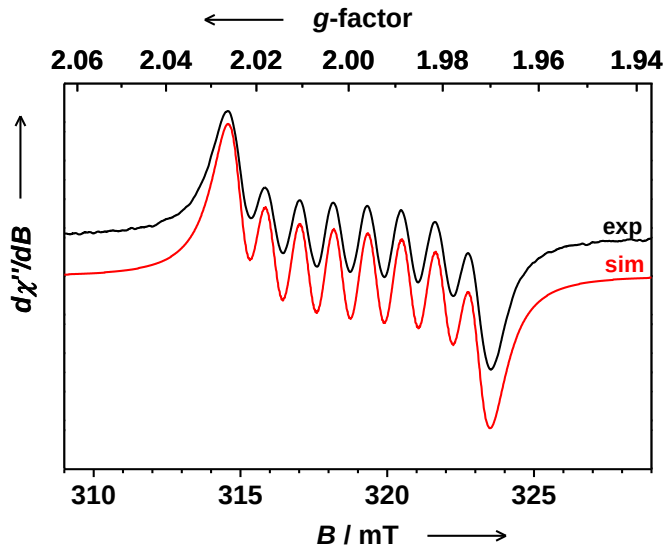

Figure S16. X-band EPR spectrum of *cis*-**6** in CH_2Cl_2 (c = 1.0×10^{-4} M) recorded at room temperature (frequency: 8.921 GHz; modulation: 0.4 mT; power: 0.1 mW). Fit parameters: g_{iso} = 1.9978, $A_{iso}(^{59}Co,\ I = 7/2) = 6.66\times10^{-3}$ cm^{-1}. Experimental spectrum is depicted by the black trace and simulation is shown in red.

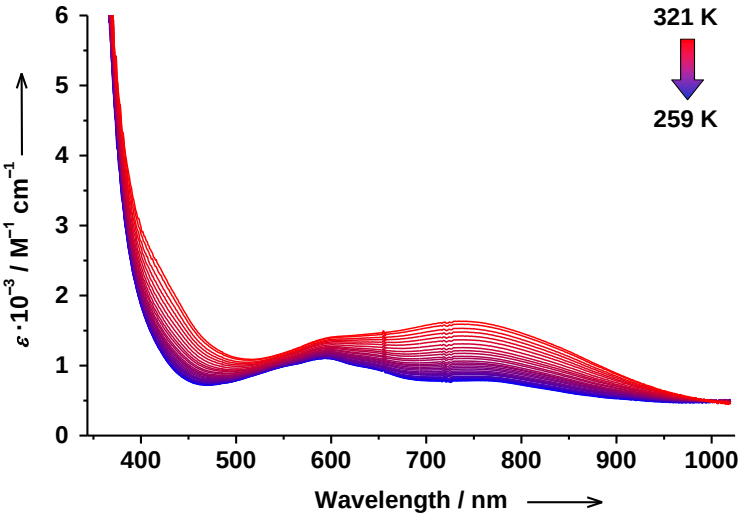

Figure S17. Temperature dependent electronic absorption spectrum of *trans*-**6** dissolved in toluene containing 12 eq of *trans*-4-styrylpyridine.

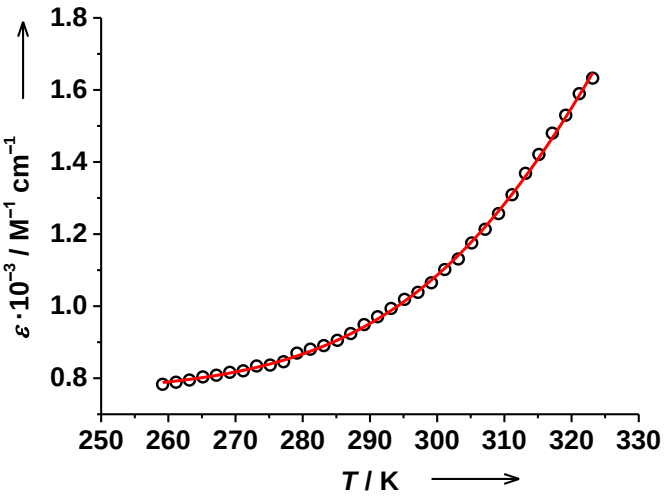

Figure S18. Temperature dependence of the 750 nm absorption band of *trans*-**6** in toluene solution containing 12 eq of *trans*-4-styrylpyridine. Van´t Hoff fit parameters: ΔH = 39(2) kJ mol^{-1}, ΔS = 108(9) J mol^{-1} K^{-1}; low- and high-temperature molar extinction coefficients: ε(LT) = 0.781(7)×10^3 M^{-1} cm^{-1} and ε(HT) = 6(1)×10^3 M^{-1} cm^{-1}. Estimated transition temperature: $T_{1/2}$ = 361 K.

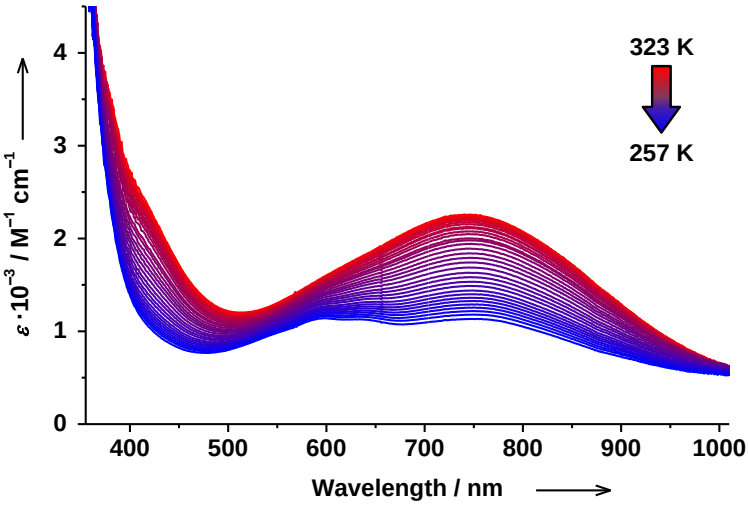

Figure S19. Temperature dependent electronic absorption spectrum of *cis*-**6** dissolved in toluene.

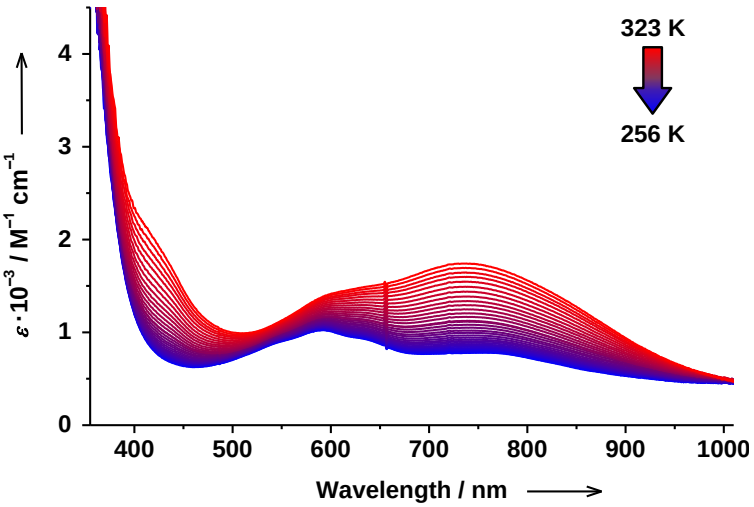

Figure S20. Temperature dependent electronic absorption spectrum of *cis*-**6** dissolved in toluene containing 20 eq of *cis*-4-styrylpyridine.

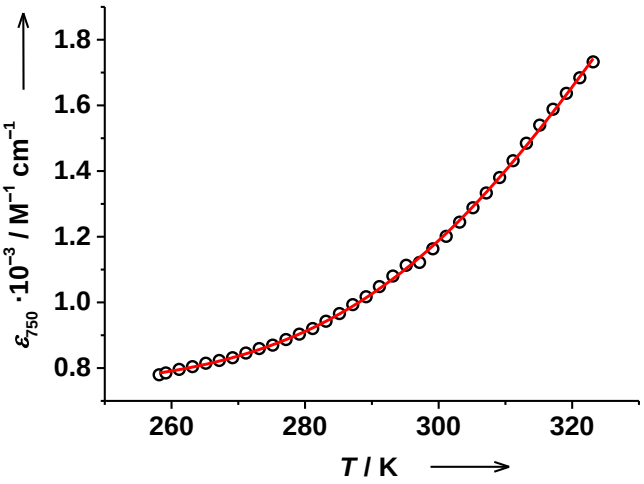

Figure S21. Temperature dependence of the 750 nm absorption band of *cis*-**6** in toluene solution containing 20 eq of *cis*-4-styrylpyridine. Van´t Hoff fit parameters: ΔH = 37(2) kJ mol^{-1}, ΔS = 110(7) J mol^{-1} K^{-1}; low- and high-temperature molar extinction coefficients: ε(LT) = 0.738(8)×10^3 M^{-1} cm^{-1} and ε(HT) = 3.6(2)×10^3 M^{-1} cm^{-1}. Estimated transition temperature: $T_{1/2}$ = 336 K.

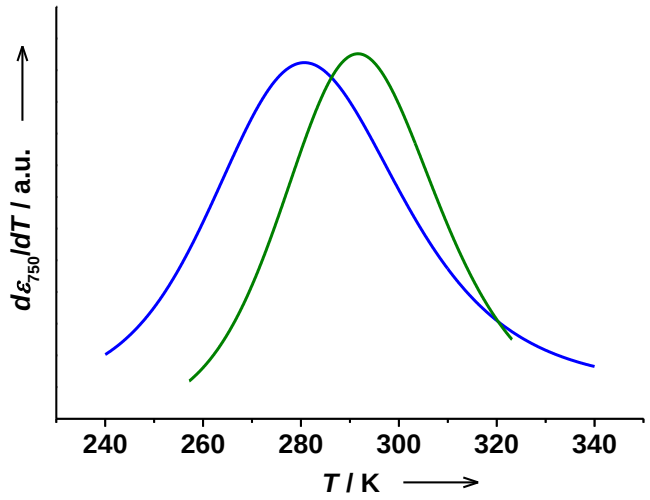

Figure S22. First derivatives of the van´t Hoff fitting curves for the temperature dependence of the 750 nm band for *trans*-**6** (green) and *cis*-**6** (blue) solutions (for original data see Figure 6 in the main text). Transition temperature $T_{1/2}$ determined by curve maximum is clearly lower for *cis*-**6** (283 K) than for *trans*-**6** (295 K).

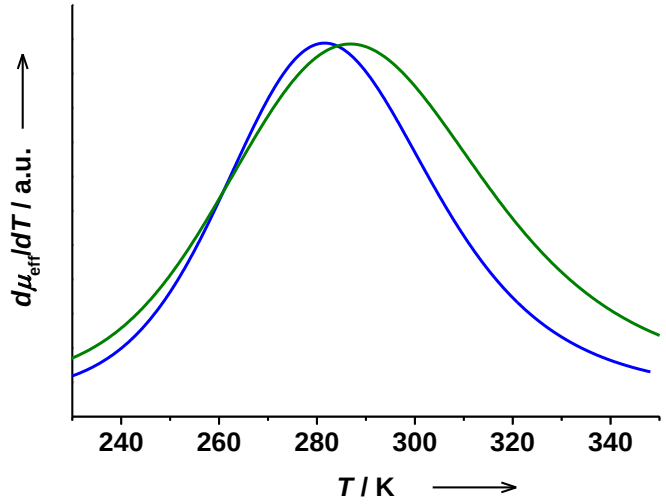

Figure S23. First derivatives of the van´t Hoff fitting curves for the temperature dependence of the effective magnetic moment for *trans*-**6** (green) and *cis*-**6** (blue) solutions (for original data see Figures 3 and 4 in the main text). Transition temperature $T_{1/2}$ determined by curve maximum is clearly lower for *cis*-**6** (288 K) than for *trans*-**6** (299 K).

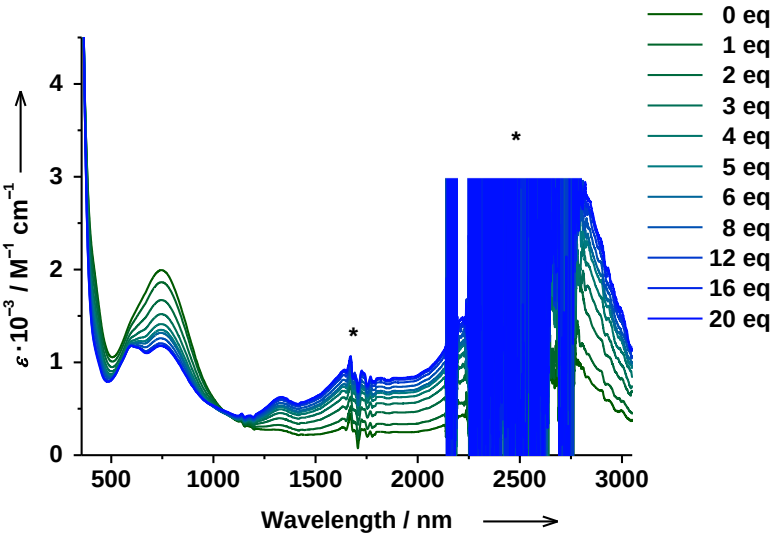

Figure S24. Changes in absorption spectrum of *cis*-**6** dissolved in toluene upon titration with *cis*-4-styrylpyridine at room temperature. Signals marked with asterix (*) are due to solvent or change of detector.

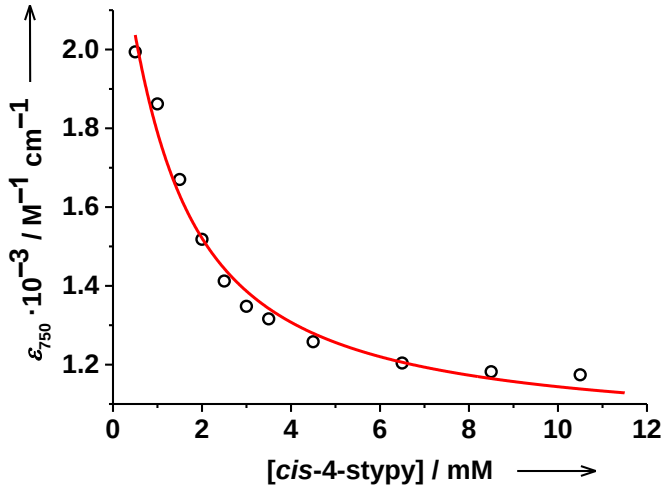

Figure S25. The evolution of the 750 nm absorption band of *cis*-**6** dissolved in toluene upon titration with *cis*-4-styrylpyridine at room temperature. Non-linear regression fit parameters: ε(*cis*-**6** ≡ {*cis*-**6**^{HS} ↔ *cis*-**6**^{LS}}) = 1.02(4)×10^3 M^{-1} cm^{-1}, ε(*cis*-**5**) = 2.4(1))×10^3 M^{-1} cm^{-1}, K_a = 1.1(3)×10^3 L mol^{-1}.

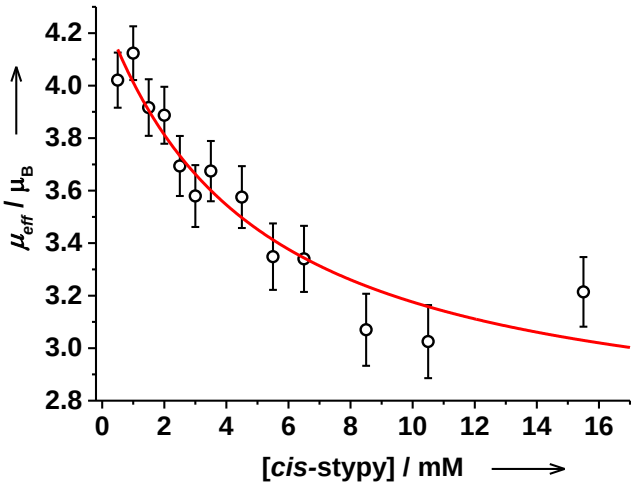

Figure S26. The evolution of the effective magnetic moment of *cis*-**6** dissolved in toluene upon titration with *cis*-4-styrylpyridine at room temperature. Non-linear regression fit parameters: μ_{eff}(*cis*-**6** ≡ {*cis*-$\mathbf{6}^{HS}$ ↔ *cis*-$\mathbf{6}^{LS}$}) = 2.4(1) μ_B, μ_{eff} (*cis*-**5**) = 4.1(3) μ_B, K_a = 0.3(1)×10^3 L mol^{-1}.

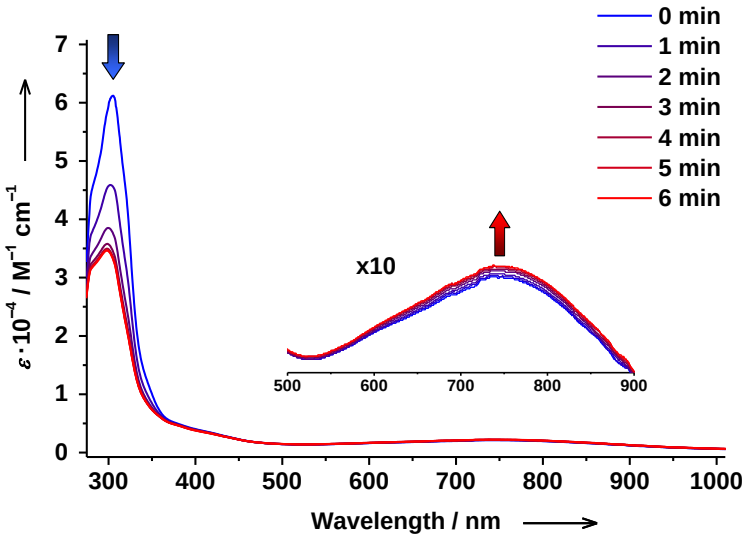

Figure S27. Changes in electronic absorption spectrum of a dilute toluene solution of *trans*-**6** upon UV irradiation at room temperature (c = 7.5×10^{-5} M, λ = 320±8 nm, 1000 W Xe lamp). The weak absorption at 750 nm is magnified.

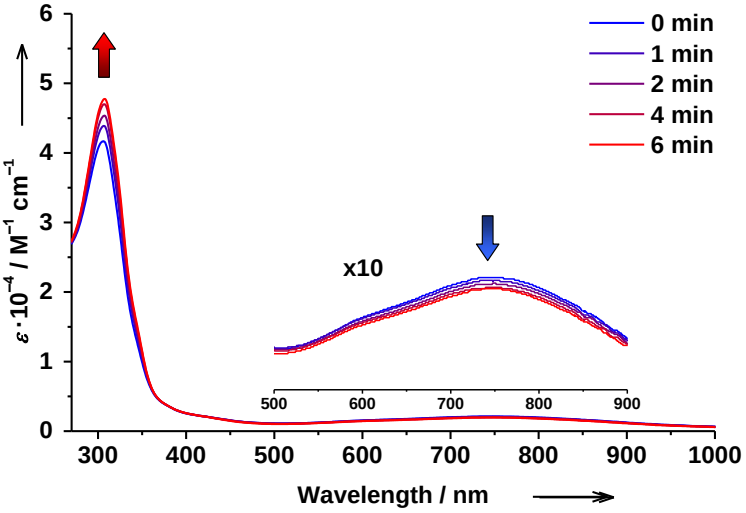

Figure S28. Changes in electronic absorption spectrum of a dilute benzene solution of *cis*-**6** upon UV irradiation at room temperature (c = 5.0×10^{-4} M, λ = 272±8 nm, 1000 W Xe lamp). The weak absorption at 750 nm is magnified.

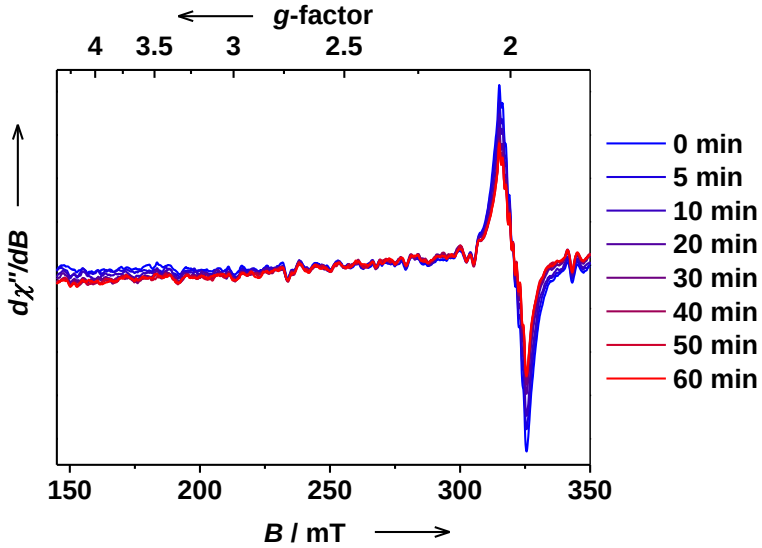

Figure S29. Changes in X-band EPR spectrum of *trans*-**6** dissolved in benzene upon UV irradiation at room temperature ($c = 1.0\times10^{-4}$ M, $\lambda = 323\pm5$ nm, 150 W Xe lamp). No new signals appeared upon irradiation.

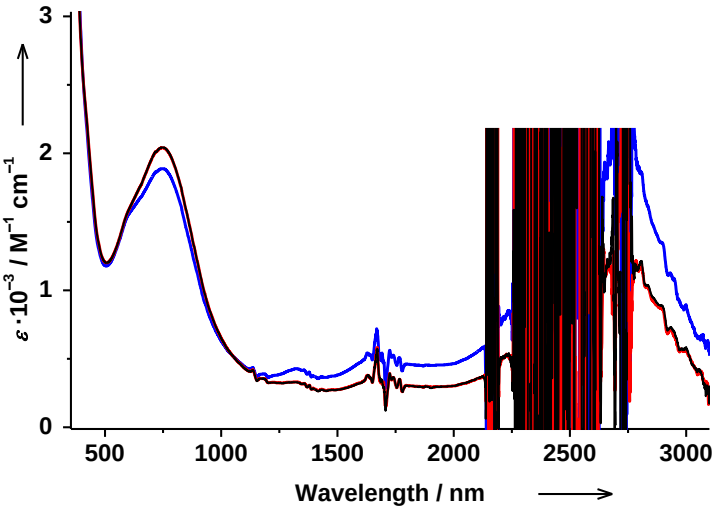

Figure S30. Thermal stability of photoinduced state: Electronic absorption spectra of *trans*-**6** dissolved in toluene ($c = 3.7\times10^{-4}$ M, room temperature) before irradiation (blue), after UV irradiation (red, $\lambda = 320\pm8$ nm, 1000 W Xe lamp), subsequently after 4 hours stored at room temperature (black).

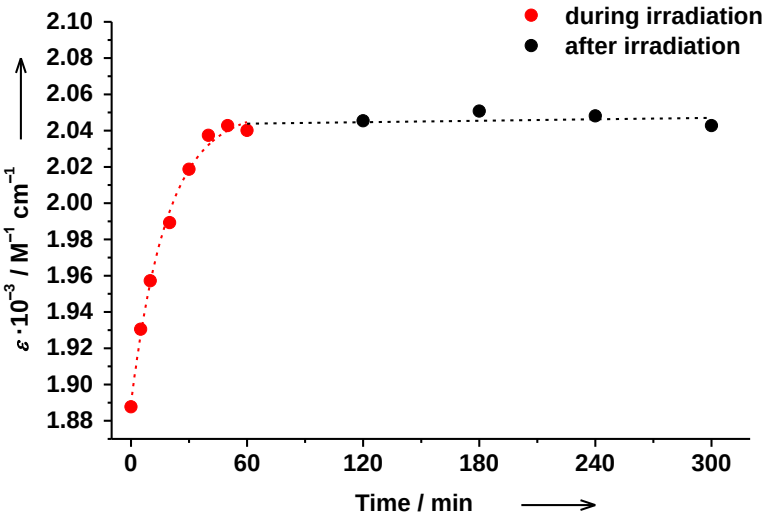

Figure S31. Thermal stability of photoinduced state: The evolution of the 750 nm absorption band of *trans*-**6** dissolved in toluene (c = 3.7×10^{-4} M, room temperature) during UV irradiation (red, λ = 320±8 nm, 1000 W Xe lamp) and after irradiation (black). Dashed lines serve as a guide to the eye.

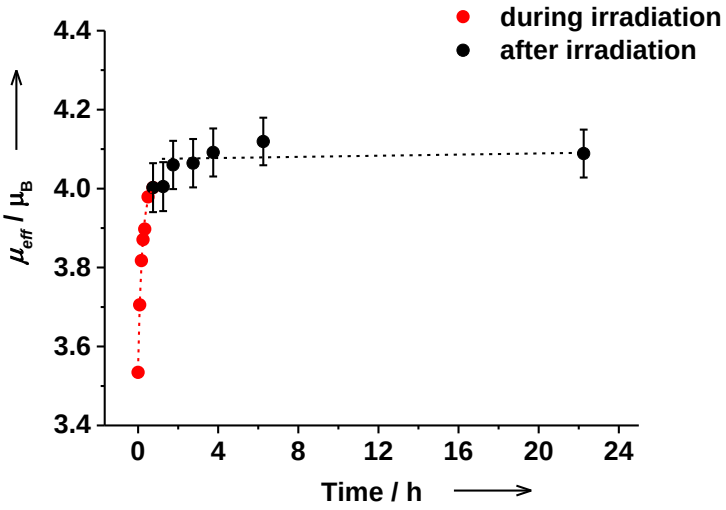

Figure S32. Thermal stability of photoinduced state: The evolution of the effective magnetic moment of *trans*-**6** dissolved in toluene during UV irradiation (red, λ = 320±8 nm, 1000 W Xe lamp) and after irradiation (black) at room temperature determined by the Evans method (c = 5.0×10^{-4} M, toluene/[D$_8$]toluene/TMS = 10:2:1). Dashed lines serve as a guide to the eye.

References

[1] G. Bain, J. Berry, *J. Chem. Educ.* **2008**, *85*, 532.
[2] R. Buchanan, B. Fitzgerald, C. Pierpont, *Inorg. Chem.* **1979**, *18*, 3439-3444.